Thermophoretic Manipulation of DNA Translocation through Nanopores

Yuhui He,[†] Makusu Tsutsui,[†] Ralph H. Scheicher,[‡] Fan Bai,[§] Masateru Taniguchi,[†,*] and Tomoji Kawai[†,*]

[†]The Institute of Scientific and Industrial Research, Osaka University, 8-1 Mihogaoka, Ibaraki, Osaka 567-0047, Japan, [‡]Division of Materials Theory, Department of Physics and Astronomy, Box 516, Uppsala University, SE-751 20 Uppsala, Sweden, and [§]Biodynamic Optical Imaging Center, Peking University, Bejing 100871, China

ABSTRACT Manipulating DNA translocation through nanopore is one crucial requirement for new ultrafast sequencing methods in the sense that the polymers have to be denatured, unraveled, and then propelled through the pore with very low speed. Here we propose and theoretically explore a novel design to fulfill the demands by utilizing cross-pore thermal gradient. The high temperature in the *cis* reservoir is expected to transform double-stranded DNA into single strands and that temperature would also prevent those single strands from intrastrand base-pairing, thus, achieving favorable polymer conformation for the subsequent translocation and sequencing. Then, the substantial temperature drop across the pore caused by the thermal-insulating membrane separating *cis* and *trans* chambers would stimulate thermophoresis of the molecules through nanopores. Our theoretical evaluation shows that the DNA translocation speeds will be orders smaller than the electrophoretic counterpart, while high capture rate of DNA into nanopore is maintained, both of which would greatly benefit the sequencing.

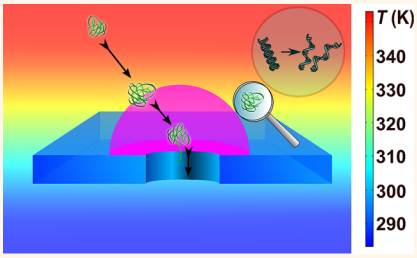

KEYWORDS: nanopore sequencing · thermophoresis · DNA capture · DNA translocation

The field of manipulating and detecting biomolecules passing through nanopores has witnessed tremendous progress over the past decade.[1−3] Among various applications, nanopore-based genome sequencing has been intensively studied with the promise of being a fast and low-cost next-generation sequencing technique.[4−6] The basic idea is to *electrophoretically* drive anionic polynucleotides into a nanopore and to discriminate each constituent nucleotide by monitoring longitudinal ionic current blockage[1−3] or transverse tunneling currents[7−10] caused by the polymer segment in the pore. For the purpose of nucleobase identifying, single-stranded DNA (ssDNA) is highly preferred rather than double-stranded (dsDNA) since the latter can only be semisequenced: the nucleotides on dsDNA thread through nanopore with a step-size of one base-pair, not one single nucleotide, which results in great difficulty to distinguish the two complementary bases on the being-interrogated pair. However, the majority of past experimental work with solid-state nanopores has been restricted to using dsDNA or very short ssDNA (≤100-mer).[11] The challenge to directly sequence longer ssDNA is the intrastrand hybridization which prevents unraveling of the coil for nanopore penetrating or leads to threading through in a multifolded manner. Another substantial difficulty is to slow down the too-fast DNA translocation motion in a nanopore during the electrophoresis.[5,6] Here the commonly used electrical approach encounters some intrinsic dilemma: a large cross-pore voltage has to be added so that the resulted electrical field around the pore entrance can capture DNA into nanopore; however, such a voltage inevitably leads to DNA translocation speed quite a few orders larger than demanded. Thereby, an efficient strategy, which can denature dsDNA, preserve the resulted ssDNA from self-hybridization, and then propel the molecules through the nanopore with sufficiently low speed would greatly benefit this research field.

Several approaches have been developed to tackle the issues. Very recent experiments report that, by locating polymerase around the pore entrance, the two complementary strands on the target dsDNA can be separated there and sequence of the single strand driven through the pore is then determined.[12,13] Nonetheless, physical approaches for DNA manipulating are usually more preferred since they are more robust and controllable toward

* Address correspondence to taniguti@sanken.osaka-u.ac.jp, kawai@sanken.osaka-u.ac.jp.

Received for review October 9, 2012 and accepted December 1, 2012.

Published online December 02, 2012
10.1021/nn304914j

the goal of mass production. In this aspect, alkaline solution with pH ~ 11.6 has been used for melting dsDNA into single strands and subsequent nanopore penetration has been detected.[14,15] Besides, by imposing additional drag force through optical[16,17] or magnetic tweezers[18] or by decreasing the electrical driving force through stronger screening of DNA charges with LiCl ions,[19] substantial decreasing of DNA translocation speeds have been reported, as reviewed by Keyser *et al.*[20] Nevertheless, a physical method capable of implementing the two tasks simultaneously, that is, denaturing DNA molecules and controlling their translocation speeds, has not emerged. A simple combination of the above techniques would be devastated by the fact that highly alkaline solution is extremely erosive and a substantial reduction of nanopore operational life under such an environment has been observed.[14]

Here in this work we propose a novel architecture that implements cross-pore temperature gradient to achieve the goals. Figure 1a demonstrates schematically the proposed design: the *cis* reservoir is kept at the melting temperature of dsDNA by an exterior heater, while the *trans* stays at a lower temperature; the nanopores are fabricated on a thermally insulating membrane connecting the two chambers. Compared to pioneering experiments manipulating thermophoresis of DNA in micro- and nanochannels,[21] the novelty and advantages of our proposed design are as follows. First, the hotter environment in the *cis* chamber would cause untwisting of dsDNA, resulting in single strands for the single-nucleotide-by-single-nucleotide identification within the pore. Then, the attained ssDNA are prevented from self-hybridization under that elevated temperature. Thereby, problems due to entangled molecule conformation, which would devastate the ensuing sequencing effort within the pore, are successfully circumvented. Last, but not the least, as plotted in Figure 1b, our calculation indicates that most of the temperature difference drops within the pore due to the presence of a heat insulating membrane. This significant temperature drop in the pore region yields a thermophoretic driving force trapping polymers into and then pulling them through the pore. That is, DNA strands are thermally propelled through the pore without the need of additional electrical driving voltage. The above analysis shows that, by utilizing a cross-pore thermal gradient, three important requisites of the nanopore sequencer, that is, denaturing dsDNA, fully unraveling the resulting single strands, and then directing the motion of DNA through the nanopore, can be fulfilled in one design. In the following we set up multiphysical models for evaluating thermophoretic translocation of DNA through nanopore, explore molecule capture and translocation mechanisms under the temperature gradient, and theoretically estimate several important quantities, like the DNA capture rates and translocation speeds.

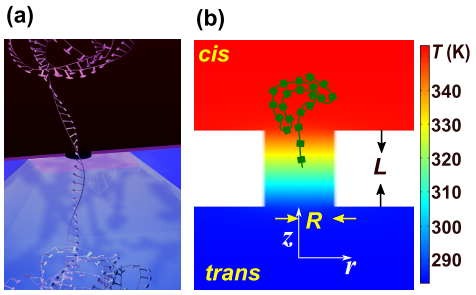

Figure 1. (a) Schematic illustration of DNA molecule translocating through nanopore under cross-pore thermal gradient. The end of the *cis* chamber is kept at the melting temperature of dsDNA T_h = 80 °C by a heater, while that of *trans* stays at room temperature T_c = 20 °C by a cooler. The membrane separating *cis* and *trans* chambers is made up of thermal insulating material so that most of the temperature difference drops around the pore. (b) Distribution of temperature in a L = 50 nm and R = 5 nm nanopore system calculated by a multiphysics model is shown with 2-D surface color in a nanopore axial and radial $z-r$ plane.

TEMPERATURE DISTRIBUTION

To assess the temperature distribution throughout the nanopore system, we first establish a multiphysical model including hydrodynamics, heat transfer, electrostatics and ionic transport (see Method) and then perform numerical calculations. The obtained temperature distribution in the $z-r$ plane for a 50 nm long and 10 nm diameter nanopore system is demonstrated in Figure 1b. Here the end of the *cis* chamber is kept at the melting temperature of dsDNA T_h = 80 °C by a heater, while that of the *trans* chamber is maintained at room temperature T_c = 20 °C by a cooler. The figure demonstrates that most of the temperature difference descends within the pore. Furthermore, as in the nanopore electrophoresis that the voltage distribution was estimated with access resistance approximation,[22,23] we develop a *thermal* access resistance model for assessing temperature distribution in our thermophoresis system as follows.

The basic idea is the resemblance between two formalisms, heat flux J_h under temperature gradient ∇T and electrical flux J_e under voltage gradient ∇V.

$$J_h = -\kappa \nabla T \quad (1)$$

$$J_e = -\sigma \nabla V \quad (2)$$

In the above expressions, κ is the thermal conductivity of the system and σ is the electrical conductivity. At steady state, the concept of electrical resistance was defined based on the second equation and the access resistance was further established for the nanopore systems.[23,24] Here we perform similar treatment by introducing the concept of *thermal* access resistance. As demonstrated in Figure 2, the *cis*/*trans* chamber is divided into two parts: the hemisphere around the pore entrance/exit (ii) and

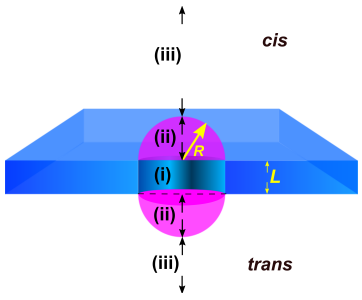

Figure 2. Thermal access resistance model for the nanopore system under temperature gradient. (i) The pore region: $(\rho_T L)/(\pi R^2)$; (ii) The hemisphere around pore entrance: $\rho_T/(4R) - \rho_T/(2\pi R)$; (iii) The outer region: $\rho_T/(2\pi R)$. Here ρ_T is an intermittent quantity defined as thermal resistivity.

the outer region (iii). The thermal resistances for (ii) and (iii) are $((\rho_T/4R) - (\rho_T/2\pi R))$ and $\rho_T/(2\pi R)$, respectively, while that for the pore region (i) is $(\rho_T L)/(\pi R^2)$. The intermittent quantity, ρ_T, is the thermal resistivity, equivalent to the electrical resistivity defined for electrical resistance. The above resistors are in a series and, thus, the temperature drop ΔT in the three regions is straightforwardly arrived at as follows:

$$(\Delta T)_i = \Delta T \frac{4L}{2\pi R + 4L}$$
$$(\Delta T)_{ii} = \Delta T \frac{\pi R - 2R}{2\pi R + 4L} \quad (3)$$
$$(\Delta T)_{iii} = \Delta T \frac{2R}{2\pi R + 4L}$$

where $\Delta T = T_h - T_c$ is the imposed temperature difference from *cis* to *trans* chamber, L is the nanopore length, and R is the pore radius. Moreover, within the pore the temperature drops nearly linearly, resulting in an almost constant temperature gradient there $(\nabla T)_i = \Delta T(1/(L + (\pi R)/2))$, while in the chambers, the temperature gradient varies inverse-quadratically with the distance from the pore ends in order to keep steady-state heat flow conserved:

$$(\nabla T)_{iii} 2\pi r^2 = (\nabla T)_i \pi R^2 \quad (4)$$

where r characterizes the distance from the pore entrance in the *cis* chamber or from the pore exit in the *trans*. Then, after some simple algebra, we obtain the temperature distribution along the nanopore axial direction as follows:

$$T(z) = \begin{cases} T_h - \Delta T \frac{R^2}{(2L+\pi R)(z-L/2)} & (z > R + L/2) \\ T_h + \Delta T \left(\frac{(\pi-2)(z-L/2)}{2\pi R+4L} - \frac{\pi R}{2\pi R+4L}\right) & (L/2 < z \le R + L/2) \\ \frac{T_h+T_c}{2} + \Delta T \frac{z}{L+\pi R/2} & (-L/2 \le z \le L/2) \\ T_c + \Delta T \left(\frac{(\pi-2)(z+R+L/2)}{2\pi R+4L} + \frac{2R}{2\pi R+4L}\right) & (-R - L/2 \le z < -L/2) \\ T_c - \Delta T \frac{R^2}{(2L+\pi R)(z+L/2)} & (z < -R - L/2) \end{cases} \quad (5)$$

In the above expression, the nanopore center is put at $z = 0$. The above analytic results show an excellent match with the numerical ones calculated by the multiphysics model given small difference between thermophoresis of cations and anions.

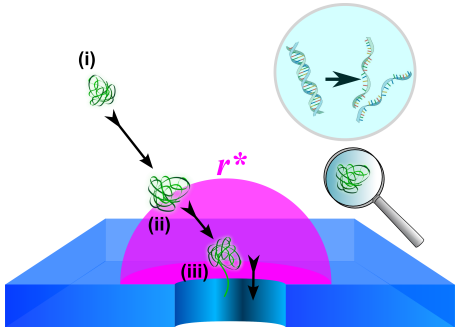

Figure 3. Sketch for DNA capture process: (i) far away from the pore entrance, thermophoresis of the polymers is negligible and DNA motion is purely diffusion; (ii) however, at distance r^* from the pore entrance, the thermodiffusion becomes sufficiently strong and dominates the polymer motion; (iii) finally, DNA molecules have to overcome an entropy barrier by putting one end into the nanopore and then initiate the penetrating process. The inset shows schematically that the dsDNA molecules get dissolved in the *cis* chamber due to high temperature there.

DNA CAPTURE KINETICS

In the bulk solution of *cis* and *trans* chambers, thermophoretic motion of molecules is described by $\vec{u} = -D_T \nabla T$, where D_T is the thermodiffusion coefficient. The counterpart of electrophoretic motion is known to be $\vec{u} = -\mu \nabla V$, where μ is the electrical mobility and V is electrical voltage. The similarity between the two formalisms triggers our idea of treating the temperature-gradient driven DNA capture kinetics in a manner akin to the voltage-gradient driven case.[25]

As shown in Figure 3, the polymer capture process involves several steps:[26,25] (i) far away from the pore entrance, DNA motion is purely diffusion while thermodiffusion is negligible, due to the fact that the temperature gradient there is almost zero $\nabla T \sim 0$; (ii) within the critical radius r^* from the pore mouth, the thermophoretic motion begins to dominate because of the rapid increasing of ∇T there; (iii) finally, when arriving at the pore entrance, one end of the polymer has to be inserted into the pore and, thus, overcomes an entropy barrier of conformation change.[26] Here the critical radius r^* is defined in analogy to the electrophoretic case:[25]

$$T_h - T(r^*) = \frac{D}{D_T} \quad (6)$$

where T_h is the high temperature rendered by the heater at the end of the *cis* chamber and D is the diffusion coefficient of ssDNA. The above equation is rewritten as $S_T(T_h - T(r^*)) = 1$ by introducing Soret coefficient $S_T = D_T/D$. Recent experiments have revealed that S_T can be derived from Gibbs free enthalpy of DNA molecules in the solution, assuming

TABLE 1. Quantities for ssDNA and dsDNA

	λ_q	l_b	r_h	l_p[a]
ssDNA	0.5 e/nt[b]	0.43 nm	$0.5((N_b l_b l_p)/3)^{1/2}$[c]	λ_D[c]
dsDNA	0.12 e/bp[d]	0.34 nm	$0.14 \times N_b^{0.75}$ nm[d]	$(((2.31 \times 10^4)/T) - 30)$ nm[e]

[a] l_p is the persistence length of polymer. [b] Data from ssDNA thermophoresis experiments,[28] while a detailed review on DNA charges within the nanopore system can be seen in ref 29. [c] Data from ssDNA FRAP experiments.[30] [d] At room temperature, data from dsDNA thermophoresis experiments.[27] [e] Data from dsDNA experiments.[31]

local thermal equilibrium:[27,28]

$$S_T = \frac{D_T}{D} = \frac{1}{kT}\frac{\partial G}{\partial T} \tag{7}$$

At room temperature or above, the Gibbs enthalpy of charged polymer is governed by the strength of shielding counterions.[27,28] Quantitatively, G is defined as follows:

$$G = \frac{Q_{eff}^2}{2\varepsilon A/\lambda_D} \tag{8}$$

where Q_{eff} is the amount of effective charges on the polymer, λ_D is the Debye length characterizing the thickness of the screening charge layer, ε is the permittivity of the solution, and A is the surface area of the polymer coil. The term $\varepsilon A/\lambda_D$ can be viewed as shielding-ion capacitance, and G is interpreted as electrical energy stored in that capacitor consisting of polymer's surface charges on one side and the shielding ions in solution on the other.[27]

In the calculation, Q_{eff} is further evaluated as $\lambda_q N_b l_b$, where λ_q is the line charge density of the DNA strand, N_b is the number of bases on that strand, and l_b is the strand contour length over base number; $A = 4\pi r_h^2$, where r_h is the hydrodynamic radius of DNA coil.[27]

Table 1 lists the quantities for ssDNA and dsDNA. For ssDNA, the relation $r_h \propto N_b^{0.5}$ results in the following expression of critical radius r^*:

$$r^* \approx \frac{3\beta\Delta T\lambda_q^2 N_b l_b R^2}{2\pi\varepsilon(2L + \pi R)} \tag{9}$$

where $\beta = -(1/\varepsilon)(\partial\varepsilon/\partial T)$. In the above derivation, the analytic expression for temperature distribution, eq 5, has been employed.

The capture rate R_c, which characterizes the throughput of nanopore sequencer, is then obtained from the following expression:[25]

$$R_c = 2\pi D r^* \tag{10}$$

DNA TRANSLOCATION KINETICS

Now we turn to investigating DNA motion within the nanopore. As seen in Figure 4, the threading-through DNA strand can be divided into three portions: the part

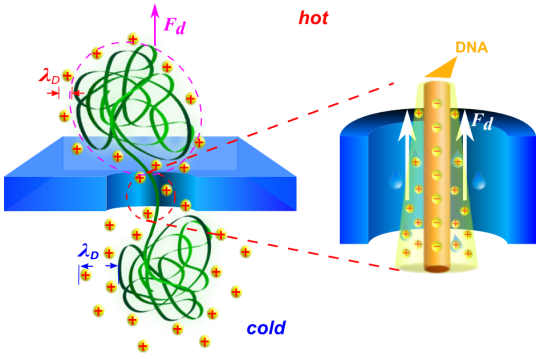

Figure 4. (a) DNA translocation stage: the surface density of Gibbs free enthalpy σ_G will decrease substantially from the hotter pore entrance to the colder exit, resulting in a Marangoni force F_m pulling DNA through the nanopore. The inset shows a DNA strand within the nanopore, where the electrical double layers undergo variation of thickness due to a substantial temperature drop there. The viscous drag force F_d within the pore and that acting on the untranslocated DNA coil are characterized by white and pink arrows, respectively.

at the pore exit that has already passed through the pore, the part that is currently inside the pore, and the part waiting to enter the pore at the entrance. Recent experiments inform us that the Gibbs enthalpy of DNA molecules is quite sensitive to the variance of temperature.[27,28] Hence, due to the significant temperature drop across the pore, the Gibbs enthalpy of DNA segments inside the pore is expected to undergo a substantial change from the pore entrance to the pore exit. However, eq 8 can no longer be used for the estimation of those DNA segments within the pore. Instead, we have to develop a cylinder model for those translocating segments, as shown in the inset of Figure 4.

The surface density of Gibbs enthalpy of DNA segments within the nanopore, σ_G, defined as the density of electrical energy stored in the cylinder capacitance, is evaluated by the following expression:

$$\sigma_G = \frac{1}{2\pi a}\int_0^{\lambda_q} \phi(\lambda)\mathrm{d}\lambda \tag{11}$$

where a is the radius of DNA single-strand, ϕ is the surface electrical potential of DNA segments, and λ_q is the line charge density on a DNA single-strand. Here we have assumed that ssDNA translocates through a solid-state nanopore in an unfolded manner, which was suggested by previous ssDNA penetrating experiments.[14] As we are going to show in the Results and Discussion, the thermodriven DNA translocation speed is orders smaller than the electrophoretic counterpart. We remind that, under such slow motion, the DNA conformation may become more complicated and there may exist a proportion of polymer passing events with a multifolded manner. For the sequencing purpose we are going to focus on the unfolded translocation events as depicted by Figure 4, while

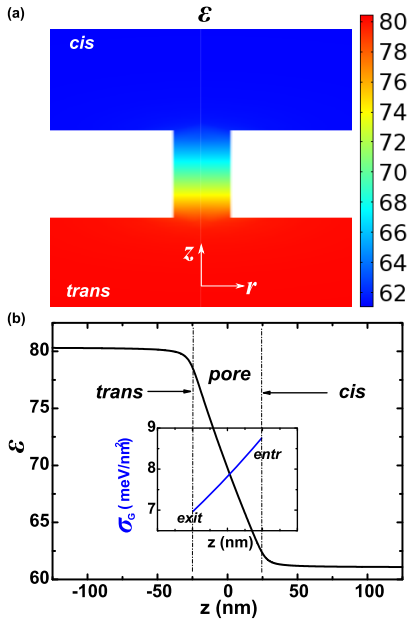

Figure 5. (a) 2-D distribution of the relative water permittivity ε in the nanopore radial−axial $r-z$ plane; (b) $\varepsilon(z)$ along the nanopore axis, while the inset plots the surface density of Gibbs enthalpy σ_G along the pore axis, where L = 50 nm and R = 5 nm.

the multifolded ones can also be assessed by tuning the quantities of effective DNA radius a and charge density λ_q in the related equations such as eq 11. $\phi(\lambda_q)$ is further calculated *via* Poisson−Boltzmann equation and its boundary conditions along the nanopore radial direction:[16,32]

$$\begin{cases} \dfrac{1}{r}\dfrac{\partial}{\partial r}\left(r\dfrac{\partial}{\partial r}\bar{\phi}\right) = \dfrac{\sinh\bar{\phi}}{\lambda_D^2} \\ \left.\dfrac{\partial\bar{\phi}}{\partial r}\right|_{r=a} = -\dfrac{\lambda_q}{2\pi a\varepsilon k_B T} \\ \left.\dfrac{\partial\bar{\phi}}{\partial r}\right|_{r=R} = 0 \end{cases} \tag{12}$$

where $\bar{\phi} = (e\phi)/(k_BT)$, $\lambda_D = ((\varepsilon k_BT)/(2C_0e^2))^{1/2}$ is the Debye length and C_0 is the imposed salt concentration. Here as a first-step investigation we have neglected the influence of surface charges on the nanopore wall.

The calculated surface density of DNA Gibbs enthalpy, σ_G, is quantitatively demonstrated in the inset of Figure 5b along the pore axis. It takes an obvious decrease from the pore entrance to the pore exit. Here we stress that the decrease of the enthalpy density is mainly attributed to the rapid raising of water permittivity ε at the lower-temperature pore exit. As seen in Figure 5, ε gets enhanced substantially from the hotter pore entrance to the colder pore exit, while it changes very little in the chambers. Such an increase results in a rapid raising of the equivalent capacitance along that axis for Gibbs enthalpy. Consequently, σ_G gets decreased along the same direction. On the other hand, as shown in the inset of Figure 4, at the colder pore exit the thickness of screening counterion layer, λ_D, in fact gets a bit larger, which would have resulted in smaller shielding-ion capacitance and, thus, increased Gibbs enthalpy density σ_G. However, that trend is overwhelmed by the fast growing of solution permittivity ε under lower temperature. The overall consequence is the reducing of Gibbs enthalpy density σ_G pointing from pore entrance to the exit.

The above analysis of σ_G indicates that DNA segments have a tendency of moving from hotter pore entrance to the colder exit. We remind that Soret coefficient or eq 7 can no longer be used here for evaluating the translocation kinetics because the temperature gradient ∇T is too large within the pore. Hereby a Marangoni force[33−35] is introduced for quantitative depiction:

$$f_m = -\frac{\partial\sigma_G}{\partial z} \tag{13}$$

and the overall thermal driving force is the integration over the pore length $F_m = 2\pi a\int_{-L/2}^{L/2} dz f_m$. The force balancing F_m is the viscous drag F_d in the solution. Generally, F_d is treated as the sum of two parts, as shown in Figure 4 and its inset: one on the untranslocated polymer coil near the pore entrance[36] and the other on the penetrating nucleotides within the pore[37]

$$F_d = \begin{cases} 6\pi\eta R_{h,c}\dfrac{dR_{h,c}}{dt} & \text{(untranslocated)} \\ \dfrac{2\pi\eta u_m L}{\ln\left(\dfrac{R}{a}\right)} & \text{(translocating)} \end{cases} \tag{14}$$

In the above expressions, η is the viscosity of water, u_m is the DNA translocation speed and $R_{h,c}$ is the hydrodynamic radius of untranslocated DNA coil in the *cis* chamber. In this work, the velocity field of the flow inside the nanopore is calculated by Navier−Stokes equation:[32]

$$\begin{cases} \eta\dfrac{1}{r}\dfrac{\partial}{\partial r}\left(r\dfrac{\partial}{\partial r}u_z\right) = \dfrac{\partial p}{\partial z} \\ u_z|_{r=a} = u_m \\ u_z|_{r=R} = 0 \end{cases} \tag{15}$$

In the above, the second and third expressions are the nonslip boundary conditions at the DNA surface and at the pore wall. Here we have neglected the viscous force on the untranslocated part since it was suggested that that force takes less than 10% of the total viscous force and moreover it keeps shrinking during the DNA translocation.[36,37] Besides, the force equation for those DNA segments inside the nanopore is written as

$$2\pi a\int_{-L/2}^{L/2} dz\,\eta\frac{\partial u_z}{\partial r}|_{r=a} = 2\pi a\int_{-L/2}^{L/2} dz\frac{\partial\sigma_G}{\partial z} \tag{16}$$

RESULTS AND DISCUSSION

Dependence of ssDNA capture rate on nanopore dimension is readily manifested in eq 10: the larger the

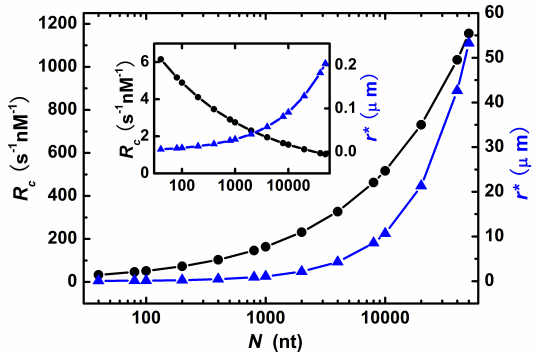

Figure 6. Calculated molecule capture rate R_c (round-symbol-black-line) and critical radius r^* (triangle-symbol-blue-line) as functions of ssDNA length N in the unit of nucleotide number (nt). Here L = 50 nm, R = 5 nm, T_h = 80 °C, T_c = 20 °C, and salt concentration C_0 = 1 mM. Inset plots the case of dsDNA in the same system except that T_h = 70 °C and T_c = 10 °C, thus, below the dsDNA melting point.

pore radius, R, or the smaller the pore length, L, the larger the critical radius, r^*, and capture rate, R_c, would be. The physical mechanism is the inverse dependence of temperature gradient $\partial T/\partial z$ on the local cross-section area A: because the heat transfer rate is conserved at the steady state $\dot{Q} = \int \vec{q} \cdot \vec{n}\, dA$, where $\vec{q}$ is the heat flux $\vec{q} \sim \partial T/\partial z$, larger pore radius R results in larger A; accordingly, the temperature gradient $\partial T/\partial z$ within the pore becomes smaller and, thus, more temperature drops outside the pore. The latter leads to reinforced polymer thermal migration toward the pore mouth, that is, increased molecule capture rate. Besides, smaller pore length L would cause smaller temperature drop inside the nanopore and in this way contributes to enhanced temperature fall in *cis* chamber, too.

Figure 6 shows the calculated capture rate of ssDNA and the related critical capture radius as functions of polymer contour length (in unit of base number). As a comparison, those of dsDNA are plotted in the inset (here the overall temperature of the system has been shifted below the melting point of dsDNA). There are two significant differences between ssDNA and dsDNA. First, given the same nanopore dimension and temperature drop across the pore, capture rate of ssDNA is two orders larger than that of dsDNA. This is attributed to the greatly reduced ssDNA coil radius when denatured from double-strand: for the same contour lengths ssDNA coil would be much smaller than dsDNA[30] and, thus, undergo substantially enhanced Gibbs enthalpy variation upon the same temperature gradient. Consequently, ssDNA acquires much stronger thermophoresis motion and thus orders of enhancement of the capture rate. Second, the variation tendency of ssDNA capture rate with the contour length is increasing, while that of dsDNA is decreasing. Here the physical mechanism is the different power-law dependence of DNA coil radiuses R_h on the strand lengths. R_h of ssDNA is subject to a slower increase with the strand length, $R_h \propto N^{0.5}$,[30] than

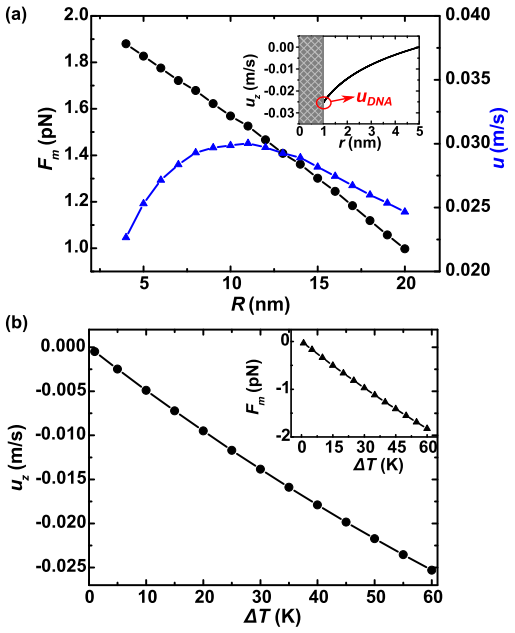

Figure 7. (a) Round-symbol-black-line shows dependence of Marangoni force F_m on nanopore radius R, while the triangle-symbol-blue-line axis shows translocation speed u. Other parameters are the same as in Figure 6. Inset plots z-component fluid velocity distribution along pore radial direction $u_z(r)$ when R = 5 nm, and the DNA velocity is marked. (b) DNA translocation speed u as a function of the imposed temperature difference ΔT. Here the elevated temperature at *cis* chamber end T_h is fixed at 80 °C, while the temperature at *trans* chamber end T_c is tuned so that $\Delta T = T_h - T_c$. Here the pore radius R = 5 nm and pore length L = 50 nm.

$R_h \propto N^{0.75}$ of dsDNA.[27] As a result, the corresponding shielding-ion capacitance $C \propto R_h^2$ of ssDNA would not increase so much as that of dsDNA, and thus, the enhancing of ssDNA Gibbs enthalpy with strand length is faster than that of dsDNA. That is, thermophoresis of ssDNA is more rapidly reinforced than that of dsDNA when strands become longer. Therefore, the capture flow of ssDNA increases with the polymer length, while dsDNA does the contrary. We remind that the predicted capture behaviors motivated by thermophoresis are profoundly different from the counterpart by electrophoresis.[25,26] Nonetheless, the calculated capture rates share similar orders with those by electrophoresis, indicating that the throughput of our thermophoretic approach is kept as that of electrical methods.

The calculated fluid velocity distribution along pore radial direction is plotted in the inset of Figure 7a where the pore radius is R = 5 nm. Due to the no-slip boundary condition, the fluid velocity at the DNA surface, that is, $r = a$, is exactly the DNA translocating velocity. Figure 7a plots Marangoni force F_m and the associated ssDNA translocation speed u as functions of nanopore radius R. The continuous decreasing of F_m with nanopore radii is attributed to the fact that larger nanopore will result in smaller temperature gradient ∇T inside the pore and, thus, smaller thermo-driving

force. Meanwhile, the molecule velocity u shows first increasing and then decreasing behavior with the varying pore radii. The physical mechanism can be found from eq 14 where the variation of viscous force F_d with pore radius R is illustrated. Being different from the almost linear decrease of F_m with R, the decreasing of viscous force is substantial when R changes from 5 to 10 nm, leading to the increasing of molecule velocity; however, that decreasing becomes more and more slow as R gets even larger. As a result, the DNA translocation velocity begins to decrease. Moreover, the calculated thermophoretic driving force is about 1−2 pN, corresponding to a cross-pore voltage of 2−4 mV in the nanopore electrophoretic experiments. Consequently, polymer translocation speeds as low as 0.02 m/s are predicted in our nanopore thermophoresis system. These are several orders smaller than those obtained by electrophoresis (∼10 m/s),[25,36,37] where much larger voltages had to be imposed. Because an effective approach of reducing DNA translocation speed is now one major challenge faced by nanopore sequencing,[5,6] our result is a great improvement over the common electrophoresis approaches. Thus, our design of nanopore thermophoresis holds a unique promise of addressing the challenge of controlling DNA transport.

Yet it is intriguing to ask the question that why the calculated thermodriven DNA translocation speed suggests an equivalent transmembrane voltage of about 2−4 mV, while on the other hand the estimated thermophoretic capture rates have to be achieved by an electrical counterpart voltage about hundreds of mV? In other words, what is the physical mechanism for having such a significant difference between thermophoresis and electrophoresis? The discrepancy is caused by the very different properties of molecule thermophoresis and electrophoresis. For the thermophoretic driving, the key word is *Gibbs enthalpy* of the molecule while for the electrophoretic counterpart that is the *charge* of the molecule. This is clearly illustrated in eqs 7 and 13 where the thermo-driving force is proportional to the grads of Gibbs enthalpy, while electrical force is known to be proportional to the charges. The Gibbs energy can be viewed as the electrical energy stored in the equivalent molecule capacitor eqs 8 and 11, and it undergoes a profound change when DNA molecule enters the pore: before entering the pore, DNA is approximated as a coil and so is the *spherical* capacitor;[25] after entering the pore, DNA segment inside the nanopore is approximated as a cylinder and so is the *cylindrical* capacitor.[38] This is visualized by comparing Figures 3 and 4. Our calculation indicates that the *energy density* stored in the cylindrical capacitor has decreased substantially compared to that stored in the spherical capacitor due to the very small diameter of DNA strands (∼2 nm). Such a reduction is the cause of much reduced thermophoretic driving force inside the nanopore. On the other hand, the *charge density* on the DNA molecules does not undergo such a change and, so, neither does the electrical driving force. Therefore, an imposed temperature difference $\Delta T \approx 60$ °C can achieve similar DNA capture rates as that by cross-pore voltage $V \sim 100$ mV, while it results in a much reduced translocation speed compared to the electrophoretic counterpart.

Though the speeds revealed here are still orders larger than the ideal value (1 base/ms ≈ 0.5 μm/s) for sequencing, there exists plenty of room for further retarding the DNA thermophoretic motion. For example, the differentiated migration of cation and anion species under thermal gradient could be utilized as *stake* or *accelerator* for the polymer motion.[39,40] It has been demonstrated that a nonuniform charge background can be induced by imposing sodium hydroxide electrolyte where OH^- is much more thermally active than Na^+, and consequently, the transport of anionic surfactant molecules is significantly retarded by such thermally induced electrical field.[40] This phenomenon suggests an approach of carefully selecting solvent electrolyte components in order to manipulate the speed of polymer thermophoretic motion over a large range. Other approaches, such as reducing the overall temperature difference ΔT by raising up the *trans* chamber temperature, can also help attenuate the thermal driving force and thus further lower the molecule translocation speed. Figure 7b plots the DNA translocation speed u as a function of the imposed temperature difference between the two chambers $\Delta T = T_h - T_c$. The speed shows a nearly linear decreasing behavior with the shrinking temperature difference. This is ascribed to the linear increase of Marangoni force with ΔT, as shown in the inset. Hence, it indicates a potential approach of slowing down DNA translocation speed by using smaller temperature gradient.

Before ending the whole discussion, we would like to draw further attention to two related issues. One is the membrane materials for real experiments, and the other is the velocity fluctuation under such low thermophoretic translocation speed. First, our modeling and discussion of DNA capture and translocation kinetics are based on the temperature distribution in a nanopore system with ideal membrane thermal insulating property. Nonetheless, in the actual circumstances, the thermal conductivity κ of the membrane is nonzero. For example, one potential candidate of thermal insulating membrane is the thin films of WSe_2 (≈32.5 nm) grown from alternating W and Se layers, of which $\kappa = 0.05$ W/m·K.[41,42] It will cause deviation of temperature distribution from ideal situation in the sense that more of the imposed temperature difference will be dropped out of the nanopore. We have simulated the temperature distribution in the nanopore system with various values of membrane thermal conductivity. The results and discussion are presented

in the Supporting Information. Second, the fluctuation of DNA motion under low translocation speed is known to be a common problem faced by the nanopore sequencing society. Here in our nanopore thermophoresis we can describe it based on overdamped Langevin equation[43] as follows

$$\gamma^* u_z = F_m + \sqrt{2k_B T\gamma^*}\,\xi(t) \quad (17)$$

where F_m is the thermo-driving force, as shown by eq 13, $\gamma^* = (2\pi\eta L)/(\ln(R/a))$ is the effective viscosity and $\xi(t)$ is the Gaussian white noise. We give some calculation and discussion in the Supporting Information for interested readers.

CONCLUSION

In summary, we have proposed the use of cross-pore temperature gradient to manipulate DNA translocation through nanopore. Our theoretical analysis has shown that preferred molecule conformation could be accomplished by the high temperature environment before entering nanopore, thus facilitating the sequencing effort within the pore. Besides, the temperature drop along the pore axis is capable of providing thermal drive sufficiently large enough to achieve high throughput and successful translocation. Some important quantities characterizing the performance of nanopore sequencer, such as DNA capture rate and translocation speed, have been evaluated by multiphysical modeling. Our calculations have demonstrated that the cross-pore thermophoresis approach can accomplish both high capture rate and orders-of-magnitude reduced translocation speed, thus, being a very promising candidate for manipulating DNA motion for the purpose of nanopore sequencing. The proposed design and analysis of nanopore thermophoresis can be further applied to the detection of uncharged or weakly charged molecules, which is difficult to be achieved by the conventional electrophoretic approach with solid-state nanopores.

METHOD

We establish a multiphysics model and perform numerical calculation for physical quantities in the nanopore solution system under temperature gradient:

$$\rho C_p\left(\frac{\partial T}{\partial t} + \vec{u}\cdot\nabla T\right) = \kappa\nabla^2 T \quad (18)$$

$$\rho\left(\frac{\partial \vec{u}}{\partial t} + \vec{u}\cdot\nabla\vec{u}\right) = -\nabla p + \eta\nabla^2\vec{u} + \vec{E}\rho_e + \vec{g}\Delta\rho \quad (19)$$

$$\nabla\cdot\vec{E} = \frac{\rho_e}{\varepsilon} = \frac{e\sum_i z_i n_i}{\varepsilon} \quad (20)$$

$$\frac{\partial n_i}{\partial t} + \nabla\cdot(-D_i\nabla n_i - n_i D_{T,i}\nabla T + \mathrm{sign}(z_i) n_i\mu_i\vec{E} + n_i\vec{u}) = 0 \quad (21)$$

The above are thermal equation for heat transfer in liquid, Navier−Stokes for hydrodynamics, Poisson for electrostatics, and generalized Nernst-Plank for ion transport. In these expressions, ρ is the water density, C_p and κ are the thermal capacitance and thermal conductivity of water, $\vec{u}$ is the fluid velocity, p is the hydrodynamic pressure, η is the viscosity of the solution, $\vec{E}$ is the electrical field within the solution, ρ_e is the net charge density caused by the difference between local cation and anion concentrations, $\vec{g}$ is the gravity vector, $\Delta\rho$ is the variation of water density due to temperature change, $\vec{g}\Delta\rho$ is the Boussinesq approximation for Navier−Stokes equation, n_i is the concentration of ith species of ions in the solution, D_i, $D_{T,i}$ and μ_i are the diffusion, thermodiffusion coefficients and electrical mobility of that ion, and z_i is the valency of the ion. The boundary of *cis* chamber is kept at high temperature $T_h = 80$ °C, while that of *trans* one is kept at low temperature $T_c = 20$ °C.

Then the two-dimensional symmetric model concerning heat transfer, hydrodynamic flow, electrostatics, and ion transport within the nanopore axial and radial $z-r$ plane was built up with COMSOL. Some very important functions, such as the quantitative dependence of water permittivity ε on temperature and Soret coefficients, $S_T = D_T/D$, come from recent experimental reports.[28,44,45] Quantitatively, they are as follows: the water viscosity $\eta(T) = 1.38 - 0.0212T + 1.36\times10^{-4}T^2 - 4.65\times10^{-7}T^3 + 8.90\times10^{-10}T^4 - 9.08\times10^{-13}T^5 + 3.85\times10^{-16}T^6$; the heat capacitance of water $C_p(T) = 1.20\times10^4 - 80.41\times T + 0.310\times T^2 - 5.38\times10^{-4}T^3 + 3.63\times10^{-7}T^4$; the thermal conductivity of water $\kappa(T) = -0.869 + 8.95\times10^{-3}T - 1.58\times10^{-5}T^2 + 7.98\times10^{-9}T^3$; the water density $\rho(T) = 838 + 1.40T - 3.01\times10^{-3}T^2 + 3.72\times10^{-7}T^3$; the relative permittivity of water $\varepsilon(T) = 78.54e^{-(4.579\times10^{-3})(T - 298.15)}$. All of the above expressions are in SI units.

Conflict of Interest: The authors declare no competing financial interest.

Acknowledgment. This research is supported partially by the Japan Society for the Promotion of Science (JSPS) through its "Funding Program for World-Leading Innovative R&D on Science and Technology". R.H.S. thanks to financial support from the Swedish Foundation for International Cooperation in Research and Higher Education (STINT) and the Swedish Research Council (VR, Grant No. 621-2009-3628).

Supporting Information Available: (1) The extra electric field generated by differentiated thermophoresis of cations and anions and its influence on DNA translocation; (2) Temperature distribution in nanopore system under various values of membrane thermal conductivity; (3) Quantitative study of translocation speed fluctuation. This material is available free of charge *via* the Internet at http://pubs.acs.org.

REFERENCES AND NOTES

1. Kasianowicz, J. J.; Brandin, E.; Branton, D.; Deamer, D. W. Characterization of Individual Polynucleotide Molecules Using a Membrane Channel. *Proc. Natl. Acad. Sci. U.S.A.* **1996**, *93*, 13770–13773.
2. Akeson, M.; Branton, D.; Kasianowicz, J. J.; Brandin, E.; Deamer, D. W. Microsecond Time-Scale Discrimination Among Polycytidylic Acid, Polyadenylic Acid, and Polyuridylic Acid as Homopolymers or as Segments Within Single RNA Molecules. *Biophys. J.* **1999**, *77*, 3227–3233.
3. Meller, A.; Nivon, L.; Brandin, E.; Golovchenko, J.; Branton, D. Rapid Nanopore Discrimination between Single Polynucleotide Molecules. *Proc. Natl. Acad. Sci. U.S.A.* **2000**, *97*, 1079–1084.
4. Zwolak, M.; Di Ventra, M. Colloquium: Physical Approaches to DNA Sequencing and Detection. *Rev. Mod. Phys.* **2008**, *80*, 141–165.
5. Branton, D.; Deamer, D. W.; Marziali, A.; Bayley, H.; Benner, S. A.; Butler, T.; Di Ventra, M.; Garaj, S.; Hibbs, A.; Huang, X.

The Potential and Challenges of Nanopore Sequencing. *Nat. Biotechnol.* **2008**, *26*, 1146–1153.
6. Venkatesan, B. M.; Bashir, R. Nanopore Sensors for Nucleic Acid Analysis. *Nat. Nanotechnol.* **2011**, *6*, 615–624.
7. Zwolak, M.; Di Ventra, M. Electronic Signature of DNA Nucleotides *via* Transverse Transport. *Nano Lett.* **2005**, *5*, 421–424.
8. Lagerqvist, J.; Zwolak, M.; Di Ventra, M.; Fast, D. N. A. Sequencing *via* Transverse Electronic Transport. *Nano Lett.* **2006**, *6*, 779–782.
9. Postma, H. W. C. Rapid Sequencing of Individual DNA Molecules in Graphene Nanogaps. *Nano Lett.* **2010**, *10*, 420–425.
10. Tsutsui, M.; Taniguchi, M.; Yokota, K.; Kawai, T. Identifying Single Nucleotides by Tunnelling Current. *Nat. Nanotechnol.* **2010**, *5*, 286–290.
11. Heng, J. B.; Aksimentiev, A.; Ho, C.; Marks, P.; Grinkova, Y. V.; Sligar, S.; Schulten, K.; Timp, G. Stretching DNA Using the Electric Field in a Synthetic Nanopore. *Nano Lett.* **2005**, *5*, 1883–1888.
12. Cherf, G. M.; Lieberman, K. R.; Rashid, H.; Lam, C. E.; Karplus, K.; Akeson, M. Automated Forward and Reverse Ratcheting of DNA in a Nanopore at 5 Å Precision. *Nat. Biotechnol.* **2012**, *30*, 344–348.
13. Manrao, E. A.; Derrington, I. M.; Laszlo, A. H.; Langford, K. W.; Hopper, M. K.; Gillgren, N.; Pavlenok, M.; Niederweis, M.; Gundlach, J. H. Reading DNA at Single-Nucleotide Resolution with a Mutant MspA Nanopore and Phi29 DNA Polymerase. *Nat. Biotechnol.* **2012**, *30*, 349–353.
14. Fologea, D.; Gershow, M.; Ledden, B.; McNabb, D. S.; Golovchenko, J. A.; Li, J. L. Detecting Single Stranded DNA with a Solid State Nanopore. *Nano Lett.* **2005**, *5*, 1905–1909.
15. Maglia, G.; Henricus, M.; Wyss, R.; Li, Q.; Cheley, S.; Bayley, H. DNA Strands from Denatured Duplexes are Translocated through Engineered Protein Nanopores at Alkaline pH. *Nano Lett.* **2009**, *9*, 3831–3836.
16. Keyser, U. F.; Koeleman, B. N.; van Dorp, S.; Krapf, D.; Smeets, R. M. M.; Lemay, S. G.; Dekker, N. H.; Dekker, C. Direct Force Measurements on DNA in a Solid-State Nanopore. *Nat. Phys.* **2006**, *2*, 473–477.
17. Keyser, U. F.; van der Does, J.; Dekker, C.; Dekker, N. H. Optical Tweezers for Force Measurements on DNA in Nanopores. *Rev. Sci. Instrum.* **2006**, *77*, 105105.
18. Peng, H.; Ling, X. S. Reverse DNA Translocation through a Solid-State Nanopore by Magnetic Tweezers. *Nanotechnology* **2009**, *20*, 185101.
19. Kowalczyk, S. W.; Wells, D. B.; Aksimentiev, A.; Dekker, C. Slowing down DNA Translocation through a Nanopore in Lithium Chloride. *Nano Lett.* **2012**, *12*, 1038–1044.
20. Keyser, U. Controlling Molecular Transport through Nanopores. *J. R. Soc. Interface* **2011**, *8*, 1369–1378.
21. Thamdrup, L. H.; Larsen, N. B.; Kristensen, A. Light-Induced Local Heating for Thermophoretic Manipulation of DNA in Polymer Micro- and Nanochannels. *Nano Lett.* **2010**, *10*, 826–832.
22. Garaj, S.; Hubbard, W.; Reina, A.; Kong, J.; Branton, D.; Golovchenko, J. A. Graphene as a Subnanometre *trans*-Electrode Membrane. *Nature* **2010**, *467*, 190–193.
23. Tsutsui, M.; Hongo, S.; He, Y.; Taniguchi, M.; Gemma, N.; Kawai, T. Single-Nanoparticle Detection Using a Low-Aspect-Ratio Pore. *ACS Nano* **2012**, *6*, 3499–3505.
24. Hall, J. E. Access Resistance of a Small Circular Pore. *J. Gen. Physiol.* **1975**, *66*, 531–532.
25. Wanunu, M.; Morrison, W.; Rabin, Y.; Grosberg, A. Y.; Meller, A. Electrostatic Focusing of Unlabeled DNA into Nanoscale Pores using a Salt Gradient. *Nat. Nanotechnol.* **2010**, *5*, 160–165.
26. Muthukumar, M. Theory of Capture Rate in Polymer Translocation. *J. Chem. Phys.* **2010**, *132*, 195101.
27. Duhr, S.; Braun, D. Why Molecules Move along a Temperature Gradient. *Proc. Natl. Acad. Sci. U.S.A.* **2006**, *103*, 19678–19682.
28. Reineck, P.; Wienken, C. J.; Braun, D. Thermophoresis of Single Stranded DNA. *Electrophoresis* **2010**, *31*, 279–286.
29. Keyser, U.; van Dorpb, S.; Lemay, S. G. Tether Forces in DNA Electrophoresis. *Chem. Soc. Rev.* **2010**, *39*, 939–947.
30. Tinland, B.; Pluen, A.; Sturm, J.; Weill, G. Persistence Length of Single-Stranded DNA. *Macromolecules* **1997**, *30*, 5763–5765.
31. Geggier, S.; Kotlyar, A.; Vologodskii, A. Temperature Dependence of DNA Persistence Length. *Nucleic Acids Res.* **2011**, *39*, 1419–1426.
32. He, Y.; Tsutsui, M.; Fan, C.; Taniguchi, M.; Kawai, T. Controlling DNA Translocation through Gate Modulation of Nanopore Wall Surface Charges. *ACS Nano* **2011**, *5*, 5509–5518.
33. Wurger, A. Thermophoresis in Colloidal Suspensions Driven by Marangoni Forces. *Phys. Rev. Lett.* **2007**, *98*, 138301.
34. Weinert, F. M.; Braun, D. Observation of Slip Flow in Thermophoresis. *Phys. Rev. Lett.* **2008**, *101*, 168301.
35. Di Leonardo, R.; Ianni, F.; Ruocco, G. Colloidal Attraction Induced by a Temperature Gradient. *Langmuir* **2009**, *25*, 4247–4250.
36. Storm, A. J.; Storm, C.; Chen, J.; Zandbergen, H.; Joanny, J.-F.; Dekker, C.; Fast, D. N. A. Translocation through a Solid-State Nanopore. *Nano Lett.* **2005**, *5*, 1193–1197.
37. van Dorp, S.; Keyser, U. F.; Dekker, N. H.; Dekker, C.; Lemay, S. G. Origin of the Electrophoretic Force on DNA in Solid-State Nanopores. *Nat. Phys.* **2009**, *5*, 347–351.
38. Ghosal, S. Effect of Salt Concentration on the Electrophoretic Speed of a Polyelectrolyte through a Nanopore. *Phys. Rev. Lett.* **2007**, *98*, 238104.
39. Wurger, A. Thermal Non-Equilibrium Transport in Colloids. *Rep. Prog. Phys.* **2010**, *73*, 126601.
40. Vigolo, D.; Buzzaccaro, S.; Piazza, R. Thermophoresis and Thermoelectricity in Surfactant Solutions. *Langmuir* **2010**, *26*, 7792–7801.
41. Chiritescu, C.; Cahill, D.; Nguyen, N.; Johnson, D.; Bodapati, A.; Keblinski, P.; Zschack, P. Ultralow Thermal Conductivity in Disordered, Layered WSe2 Crystals. *Science* **2007**, *315*, 351.
42. Chiritescu, C.; Cahill, D. G.; Heideman, C.; Lin, Q.; Mortensen, C.; Nguyen, N. T.; Johnson, D.; Rostek, R.; Botner3, H. Low Thermal Conductivity in Nanoscale Layered Materials Synthesized by the Method of Modulated Elemental Reactants. *J. Appl. Phys.* **2008**, *104*, 033533.
43. Reimann, P.; Meyer, A.; Getfert, S. On the Lubensky-Nelson Model of Polymer Translocation through Nanopores. *Biophys. J.* **2012**, *103*, 889–897.
44. Agar, J. N.; Mou, C. Y.; Lin, J. L. Single-Ion Heat of Transport in Electrolyte Solutions: A Hydrodynamic Theory. *J. Phys. Chem.* **1989**, *93*, 2079–2082.
45. Majee, A.; Wurger, A. Collective Thermoelectrophoresis of Charged Colloids. *Phys. Rev. E* **2011**, *83*, 061403.